Chapter 4.4

The Virtual Electrode Hypothesis of Defibrillation

Crystal M. Ripplinger and Igor R. Efimov

Introduction

Despite significant research efforts of investigators in academia, medicine, and the pharmaceutical industry, no effective pharmacological alternative to defibrillation by electric shock has been developed. Thus, defibrillation has evolved to become the only effective therapy against sudden cardiac death. Highly detailed knowledge of ion channel biophysics and cell signaling cascades has allowed for the development of numerous specific agonists and antagonists, but as of yet, has failed to deliver safe and effective antiarrhythmic therapy. In contrast to this approach, electrotherapy is steadily improving its efficacy and safety.

Despite major improvements over the past several decades, defibrillation is not free from side effects, which may include both contractile and electrical dysfunction.[1–3] In addition to physical damage to the heart, defibrillation is also associated with psychological side effects.[4,5] Therefore, reduction of defibrillation energy is highly desirable. However, the basic mechanisms of defibrillation still remain debatable a century after its inception, which has slowed further improvement of the therapy. This chapter explores one of the leading hypotheses of defibrillation, the virtual electrode hypothesis, which has emerged over the past decade through the successes of novel research methodologies, including optical mapping and bidomain modeling.

Historical Overview of Defibrillation Therapy

The motivation to explore the relationship between electrical activity of the heart and that of external electric stimuli began in the late nineteenth century, presumably due to the increasing electrification of urban areas.[6] In 1899, while studying induction of ventricular fibrillation in the dog heart, physiologists Prevost and Batelli working at the University

Igor R. Efimov
Department of Biomedical Engineering, Washington University, St. Louis, MO, USA, igor@wustl.edu

I. R. Efimov et al. (eds.), *Cardiac Bioelectric Therapy: Mechanisms and Practical Implications.*

of Geneva discovered that they could defibrillate a dog heart by applying an appropriate high current shock directly to the surface of the myocardium: "We have shown that the fibrillatory tremulations produced in the dog, in which they are definitely established can under certain circumstances be arrested, the heart re-established its beats, if one submits the animal to passages of a high current of high voltage (of 4800 volts, for example)."[7]

In 1946 Russian physiologists Gurvich and Yuniev[8] reported defibrillation of the mammalian heart, with a capacitor discharge applied externally across the closed chest. The next year Beck et al.[9] reported the first successful human defibrillation in which they used two 110-V, 1.5-A alternating current (AC) current shocks to resuscitate a 14-year-old boy who suffered cardiac arrest during elective chest surgery. In 1956 Zoll et al.[10] performed the first successful human external defibrillation using a 15-A AC current that produced 710 V applied across the chest for 0.15 s. However, the superiority and safety of direct current (DC) over AC for defibrillation were demonstrated by several investigators such as Kouwenhouven and Milnor,[11] Lown et al.,[12] and Gurvich.[13] In 1969 Mirowski et al.[14,15] began research on the implantable cardioverter-defibrillator (ICD). In 1980 the first ICD was implanted in a human patient at Johns Hopkins Hospital. Since the advent of ICD technology, survival for those at high risk for ventricular tachycardia/fibrillation (VT/VF) has greatly improved.

Despite profound advancements in defibrillation therapy over the past century, little was known about the basic mechanisms of defibrillation until the past two decades due to the advent of fluorescent optical mapping with voltage-sensitive dyes. In parallel, advancements in numerical simulations using the bidomain model of cardiac tissue provided the theoretical means to interpret these complex experimental findings.

Bidomain Model

The bidomain model is now widely accepted for numerical and theoretical studies of cardiac electrophysiology. The tissue is represented by two interpenetrating intra- and extracellular domains with each of them having different conductivities along and across the direction of the fibers.[16,17] The state variables describing the system are intracellular (ϕ_i) and extracellular (ϕ_e) potentials defined everywhere in the domain of interest Ω. The transmembrane potential is defined as $V_\mathrm{m} = \phi_\mathrm{i} - \phi_\mathrm{e}$. The following coupled reaction-diffusion equations constitute the bidomain model:

$$\nabla \cdot (\hat{\sigma}_\mathrm{i} \nabla \phi_\mathrm{i}) = I_\mathrm{m}, \tag{1}$$

$$\nabla \cdot (\hat{\sigma}_\mathrm{e} \nabla \phi_\mathrm{e}) = -I_\mathrm{m} - I_\mathrm{o}, \ \text{ in}\,\Omega, \tag{2}$$

where $\hat{\sigma}_\mathrm{i}$ and $\hat{\sigma}_\mathrm{e}$ are intra- and extracellular conductivity tensors, respectively, I_m is the volume density of transmembrane current, and I_o is the volume density of the stimulation or shock current.

The transmembrane current is described as a sum of capacitive, ionic, and electroporation currents[18]:

$$I_\mathrm{m} = \beta \left(C_\mathrm{m} \frac{\partial V_\mathrm{m}}{\partial t} + I_\mathrm{ion}(V_\mathrm{m}, t) + G(V_\mathrm{m}, t) \cdot V_\mathrm{m} \right), \tag{3}$$

where β is the surface-to-volume ratio (total membrane area divided by total tissue volume), C_{m} is the membrane capacitance, and $G(V_{\mathrm{m}}, t)$ is the electroporation conductance, which can be described by empirical equations.[19]

The ionic current, $I_{\mathrm{ion}}(V_{\mathrm{m}}, t)$, depends on the model of the cardiac myocyte used and can range from relatively simple and therefore less accurate (Beeler-Reuter,[20] BRDR[21]) to more complex (Luo-Rudy phase I[22] or II,[23] Hund-Rudy dynamic model[24]). These models describe individual ion channels kinetics and are based on Hodgkin-Huxley formalism.[25]

Fluorescent Optical Mapping

The development of optical recordings of membrane potential was driven by the need to overcome many obstacles in electrophysiology and the promise of a technology "for measuring membrane potential in systems where, for reasons of scale, topology, or complexity, the use of electrodes is inconvenient or impossible."[26] Based on our current experience in cardiac electrophysiology, this list needs to be extended to recordings of action potentials in the presence of external electric fields during stimulation and defibrillation; an impossible task with both extra- and intracellular electrodes due to the large electrical artifacts caused by external fields. Optical mapping techniques and potentiometric probes have now made major contributions to our understanding of cardiac electrophysiology in ways that could not have been accomplished with other approaches.

Over 30 years ago, investigators discovered molecular probes that bind to the plasma membrane of neuronal[27] and cardiac cells[28] and exhibit changes in fluorescence and/or absorption that mimic changes in transmembrane potential. Thus, the transmembrane potential can be measured by illuminating tissue stained with the fluorophore and detecting changes in the intensity or wavelength of the emitted light. Several useful classes of fluorophores have emerged over the past 30 years, including merocyanine, oxonol, and styryl dyes. However, styryl dyes represent the most popular family of dyes for cardiac electrophysiology applications, with RH-421 and di-4-ANEPPS being the most prominent members of this family. The spectroscopic properties of these dyes have been shown to have a linear response to transmembrane potential changes in the normal physiological range.[29–31]

The typical optical mapping experimental setup consists of an isolated tissue preparation or Langendorff-perfused heart that is perfused and/or superfused with an oxygenated physiologic crystalloid solution. The heart is stained with the voltage-sensitive fluorophore and illuminated with light at the correct excitation wavelength. The excitation light can be produced with lasers,[32] tungsten-halogen lamps,[28] or more recently with light emitting diodes (LEDs).[33–35] The emission light is filtered and can be collected by a charge-coupled device (CCD) camera, complementary metal-oxide semiconductor (CMOS) camera, or a photodiode array (PDA). The optical signals are typically digitized at 1–5 kHz and normalized, and two-dimensional maps of propagation can then be constructed. Many groups are now using one[36–38] or two[39] optical detectors in combination with a panoramic mirror arrangement, or three[40] optical detectors to record electrical activity on the entire surface of the heart and reconstruct propagation in three dimensions.

Virtual Electrodes and the Activating Function

The term *virtual electrode* was coined by Seymour Furman to explain the clinical observation of stimulation far from a chronically implanted pacemaker lead.[41] Later, this term was adopted by investigators studying both pacing and defibrillation in parallel with a synonymous but more rigorously defined term *activating function* to designate the "driving force," which drives transmembrane potential in either a depolarizing (positive) or hyperpolarizing (negative) direction following an externally applied electric field. The bidomain equations (1)–(2) can be rewritten in terms of the transmembrane ($V_m = \phi_i - \phi_e$) and extracellular (ϕ_e) potentials:

$$\nabla \cdot ((\hat{\sigma}_i + \hat{\sigma}_e)\nabla\phi_e) = -I_o - \nabla \cdot (\hat{\sigma}_i \nabla V_m), \tag{4}$$

$$I_m - \nabla \cdot (\hat{\sigma}_i \nabla V_m) = \nabla \cdot (\hat{\sigma}_i \nabla \phi_e). \tag{5}$$

During diastole, one can neglect the gradient of transmembrane potential in the left-hand side of (5) as well as the total transmembrane current. Therefore, the only source of transmembrane potential changes is the term in the right-hand side of (5), which is known as the generalized activating function:[42,43]

$$S = \nabla \cdot (\hat{\sigma}_i \nabla \phi_e) = \hat{\sigma}_i \Delta \phi_e + \nabla \hat{\sigma}_i \cdot \nabla \phi_e. \tag{6}$$

Quantitative investigation of virtual electrodes and the activating function started with the theoretical predictions of Sepulveda et al.,[44] who demonstrated that a unipolar stimulus produces both positive and negative polarization in a two-dimensional syncytium. These positive and negative polarizations are induced by virtual cathodes and virtual anodes, respectively.[45] The magnitude and location of positive and negative virtual electrodes depend on both the field configuration (ϕ_e) and tissue structure (σ_i and σ_e).[43]

These findings explained the phenomenon of anodal stimulation, which had eluded investigators for many years. According to classical cable theory, anodal stimulation hyperpolarizes tissue and thus cannot bring about an action potential. However, experimentalists had long observed excitation as a result of anodal stimulation. The virtual electrode theory predicts that virtual anodes are accompanied by virtual cathodes; therefore, action potentials can arise from these regions.

Early theories of predicted efficacy of defibrillation shocks were entirely based on the minimum external voltage gradient ($\nabla\phi_e$). As evident from the definition of the activating function (6), voltage gradient ($\nabla\phi_e$), while important, is not the only source of membrane polarization. Tissue structure (σ_i and σ_e) may be just as important. Microscopic and macroscopic tissue heterogeneities play an important role by providing the substrate for virtual electrodes during defibrillation shocks. What remains to be determined is the relative contribution of different scales of heterogeneities to defibrillation. Some groups argue that microscopic cell-size heterogeneities play the major role,[46] while other groups are convinced that large-scale heterogeneities are more important, because of the averaging effect of small-scale virtual electrodes by electrotonic interaction.[47]

Mechanisms of Defibrillation

In order to terminate an arrhythmia by electric shock, the shock must (1) terminate all or most wavefronts that sustain VT/VF; (2) not reinduce VT/VF; (3) suppress sources of VT/VF if they are focal in nature; and (4) not suppress postshock recovery of the normal sinus rhythm.

Theories of Defibrillation

In 1899 when Prevost and Battelli[7] discovered that large electric shocks could defibrillate the fibrillating myocardium, they posed the first theory of defibrillation, which was based on the "incapacitation" effects on the myocardium of strong electric shocks. It was not until 1939 that Gurvich and Yuniev proposed the first stimulatory theory of defibrillation.[48] They postulated directly stimulating and exciting the myocardium achieved defibrillation.

The stimulatory theory of defibrillation was later refined into the critical mass hypothesis in which experimentalists as well as theorists proposed that a critical mass of the myocardium (75–90%) needs to be directly defibrillated in order to fully terminate fibrillation.[49–51] This theory stated that the remaining fibrillating areas not affected by the shock would self-terminate.

In 1967 Fabiato and colleagues[52] demonstrated the first correlation between shock-induced fibrillation and defibrillation in a mechanism they called the "threshold of synchronous response." This idea was later extended by Chen and co-workers[53] into the now well-known "upper limit of vulnerability" hypothesis. This hypothesis states that the shock must terminate all wavefronts of fibrillation and that, in order to be successful, the shock must produce a sufficient voltage gradient (above the upper limit of vulnerability [ULV]) everywhere in the myocardium as not to reinduce fibrillation. This correlation was subsequently demonstrated in several experimental studies[54,55] and in humans.[56,57]

Although the concept of stimulus-induced reentry had been laid down decades earlier by Wiener and Rosenblueth,[58] Frazier and colleagues[59] were the first to obtain experimental evidence of this mechanism in 1989 in what they called the "stimulus-induced critical point" mechanism. Frazier et al. demonstrated that the chirality of reentry could be predicted based on the direction of the preshock repolarization gradient and the voltage gradient of the applied shock. After its discovery, the critical point mechanism was held responsible for reinduction of fibrillation after a failed defibrillation shock.[60,61]

In 1998 Dillon and Kwaku[62] proposed the "progressive depolarization" hypothesis of defibrillation and shock-induced fibrillation. This theory expanded on the critical mass, threshold of synchronous response, and ULV hypotheses but with a different interpretation of the supporting experimental evidence. The progressive depolarization hypothesis states that: "(1) Progressively stronger shocks depolarize, (2) Progressively more refractory myocardium, to (3) Progressively prevent postshock wavefronts, and (4) Prolong and synchronize post-shock repolarization, in a (5) Progressively larger volume of ventricle, to (6) Progressively decrease the probability of fibrillation after the shock." Thus, this theory is based on the prolongation of repolarization and refractory periods to effectively eliminate the excitable gap and terminate fibrillation.

However, contrary to this hypothesis, theoretical and experimental evidence supports the creation of virtual electrodes of opposite polarity in response to an applied stimulus.[44,45,63–66] Although the shock may prolong repolarization in some regions of the myocardium, it may be shortened in others. Thus, the virtual electrode mechanism casts doubt on all of the previously outlined theories of defibrillation, as these theories only account for the "stimulatory" response of defibrillation shocks. An alternative theory that accounts for both shock-induced excitation and deexcitation is the virtual electrode hypothesis of defibrillation.[66–68]

Virtual Electrode Hypothesis of Defibrillation: The Role of Deexcitation and Reexcitation

The virtual electrode hypothesis was the first to account for shock-induced deexcitation in both the mechanisms of defibrillation and shock-induced reentrant arrhythmias. When cardiac tissue is exposed to external field stimulation, areas of the tissue can be depolarized or hyperpolarized. Depolarization can result in prolongation of the action potential if the tissue is refractory (Fig. 1, middle trace) or activation if the tissue is excitable. Hyperpolarization can shorten the action potential and completely repolarize the tissue (Fig. 1, top trace) to restore excitability. This phenomenon is often referred to as "deexcitation" and is an all-or-none response. In addition, deexcitation may be followed by reexcitation caused by a postshock propagating wave (Fig. 1, bottom trace).

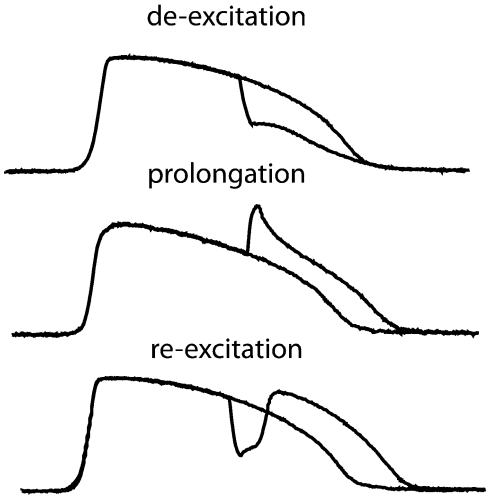

Figure 1: Tissue responses to virtual electrode polarization. The virtual anode deexcites the tissue and shortens the action potential and refractory period. The virtual cathode extends the action potential duration and refractory period. If deexcitation fully or partially restores excitability in the area of the virtual anode, and if the virtual cathode is within one space constant, reexcitation will take place

Further illustration of simultaneous shock-induced prolongation and shortening of the action potential is shown in Fig. 2.[69] The top panels of Fig. 2a show maps of postshock (+200 V) transmembrane potential (left), and action potential duration during a control beat (middle) and postshock (right). The action potentials were shortened in areas of negative polarization and prolonged in areas of positive polarization, resulting in dispersion of repolarization. In contrast, Fig. 2b shows a response that appears as action potential prolongation in all areas when the shock voltage was increased to +300 V. There is little difference in the areas of positive polarization (red traces), but dramatic differences in the areas of negative polarization (blue traces). In these areas, action potentials were shorted with a +200 V shock and lengthened due to reexcitation in response to a +300 V shock.

Virtual Electrode-Induced Phase Singularity Mechanism

Shock-induced arrhythmias were discovered over 150 years ago by Hoffa and Ludwig.[70] Since that time, experimentalists and theorists alike have investigated the relationship between defibrillation and shock-induced arrhythmogenesis. We can assume that shocks initiate arrhythmias via reentry, and that defibrillation shocks fail because they either leave fibrillating myocardium unaffected by the shock or because they produce a new reentrant arrhythmia. Therefore, it is relevant to discuss shock-induced arrhythmias in the settings of the virtual electrode hypothesis of defibrillation.

It is known that shocks delivered to refractory myocardium can induce reentry via break excitation.[67,71,72] Figure 3 shows how the postshock virtual electrode pattern can lead to reentry.[67] Figure 3a shows the postshock virtual electrode polarization (VEP). Deexcitation occurred only in the most negatively polarized region near the bottom right corner of the field of view. After the shock, the positively polarized region interacted electronically with the deexcited region (break excitation) to create a new wavefront that propagated from left to right (Fig. 3b). This new wavefront of activation then propagated slowly upward into the recovering myocardium to create a reentrant circuit (Fig. 3c). The circle in Fig. 3a indicates the point of shock-induced phase singularity[73] responsible for the initiation of reentrant activity.

It was subsequently demonstrated by Cheng et al.[69] that creation of reentrant arrhythmias via the virtual electrode-induced phase singularity mechanism is critically dependent on the magnitude of the applied electric field. Figure 4 shows examples of postshock VEP and resulting patterns of activation in response to an −80 (Fig. 4a), −160 (Fig. 4b), and −220 V (Fig. 4c) shocks. In Fig. 4a, complete deexcitation occurred only in the most negatively polarized region in the bottom right corner (darkest blue). As illustrated in the corresponding activation map, this region was excited first, followed by slower excitation spreading upward as these areas recovered. Excitation then spread to the left of the field of view producing a reentrant wavefront. At larger shocks strengths (Fig. 4b, c), larger regions were completely deexcited by the shock (darkest blue). Thus, a wavefront of reexcitation was produced in a larger area, promptly exciting the entire deexcited region. Such fast excitation does not allow for recovery of the incompletely deexcited regions; therefore, reentry is not produced in these cases. Thus, conduction velocity of the postshock wavefront depends on the magnitude of VEP (degree of shock-induced deexcitation).

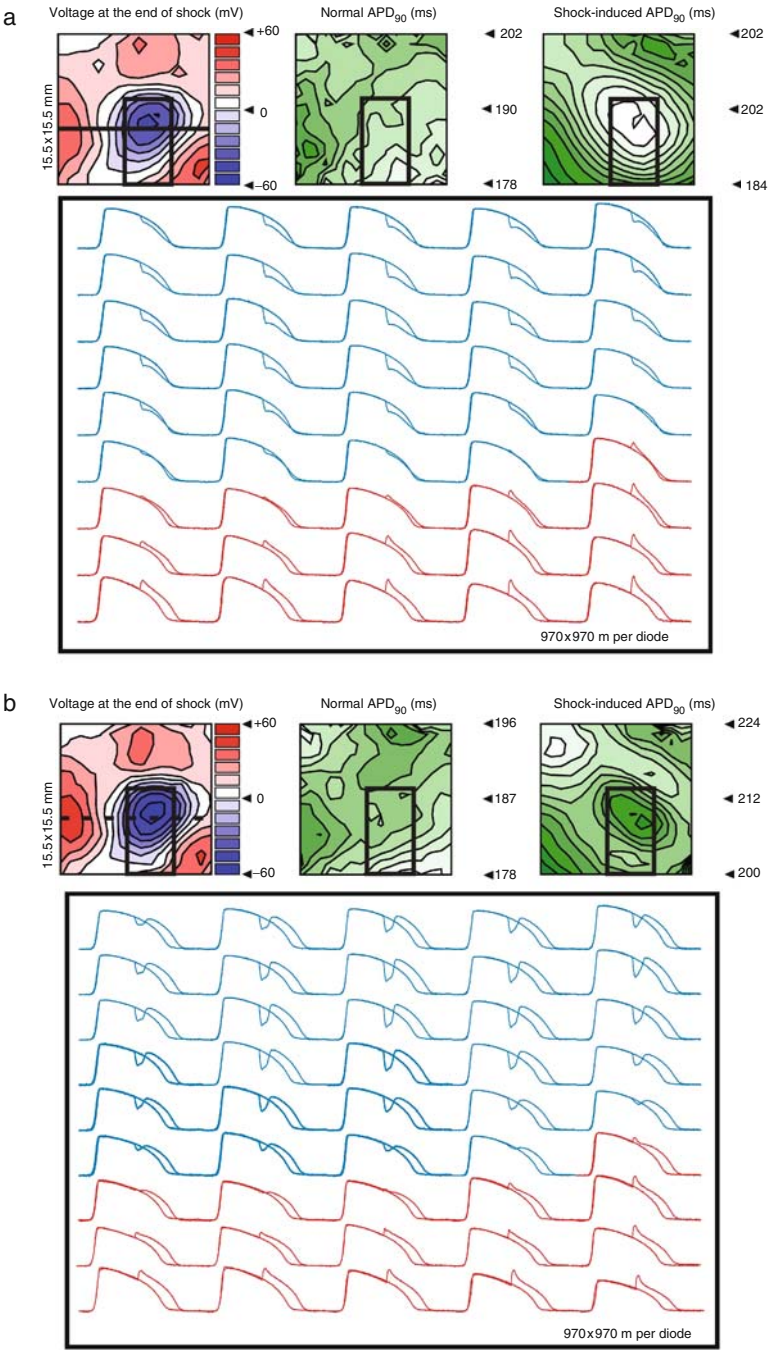

Figure 2: Simultaneous negative and positive polarizations induced by a monophasic anodal shock. (**a**) Response to a +200 V shock, which produced a high degree of dispersion of repolarization. (**b**) Response to a +300 V shock, which prolonged action potential duration everywhere in the region of interest. See text for details (Cheng et al. 1999)[69]

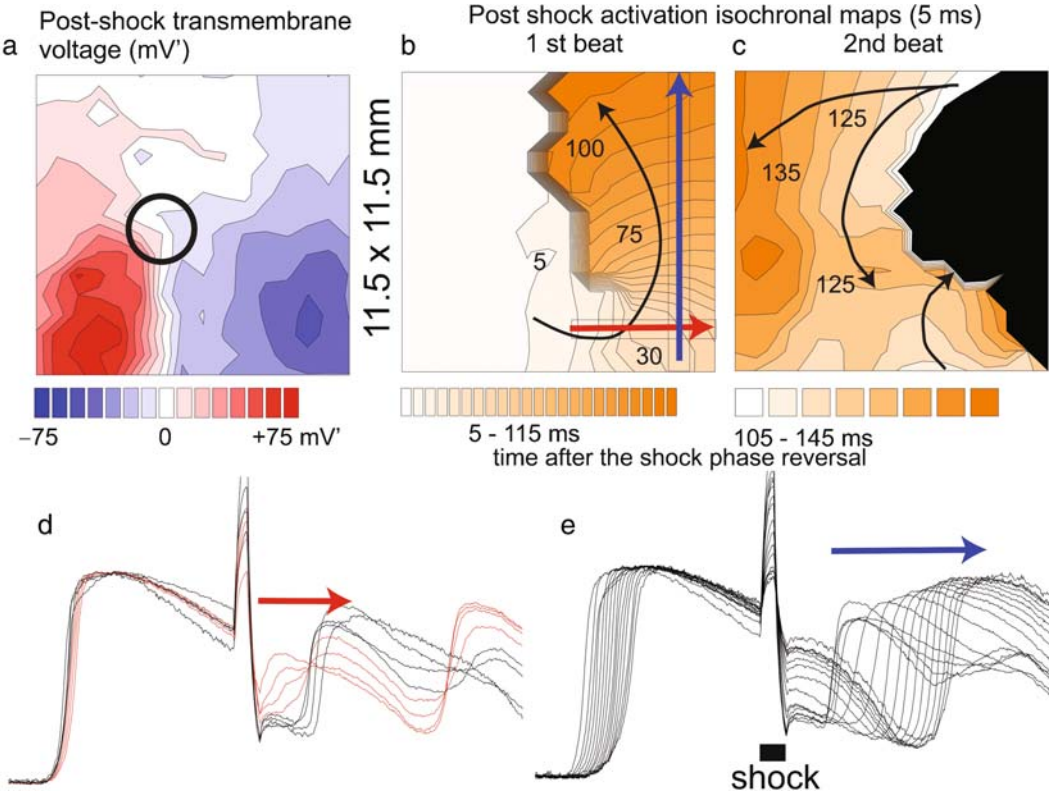

Figure 3: Virtual electrode-induced phase singularity mechanism. (**a**) Postshock pattern of virtual electrode polarization (VEP). (**b**) Immediately postshock, activation spreads to the deexcited region in the lower right corner and proceeds upward into the recovering myocardium to create a reentrant circuit (**c**). (**d**) Optical recordings from eight sites marked with the red arrow in (**b**). (**e**) Optical recordings from 16 sites marked with the blue arrow in (**b**) (Efimov et al. 1998)[67]

Presumably, the stronger negative polarization results in more complete recovery of sodium channels from inactivation and, therefore, faster conduction of postshock reexcitation. This relationship between conduction velocity and negative polarization is now thought to underlie the mechanisms of the upper and lower limits of vulnerability.[74] Low-intensity shocks producing inadequate negative polarization will result in failure of postshock conduction and, thus, failure to produce phase singularities. High-intensity shocks will produce a strong gradient of polarization, resulting in supernormal conduction, immediately extinguishing the excitable gap. Only shocks of "moderate" magnitude will produce conduction velocities appropriate for the creation of phase singularities and reentrant arrhythmias as in Fig. 4a.

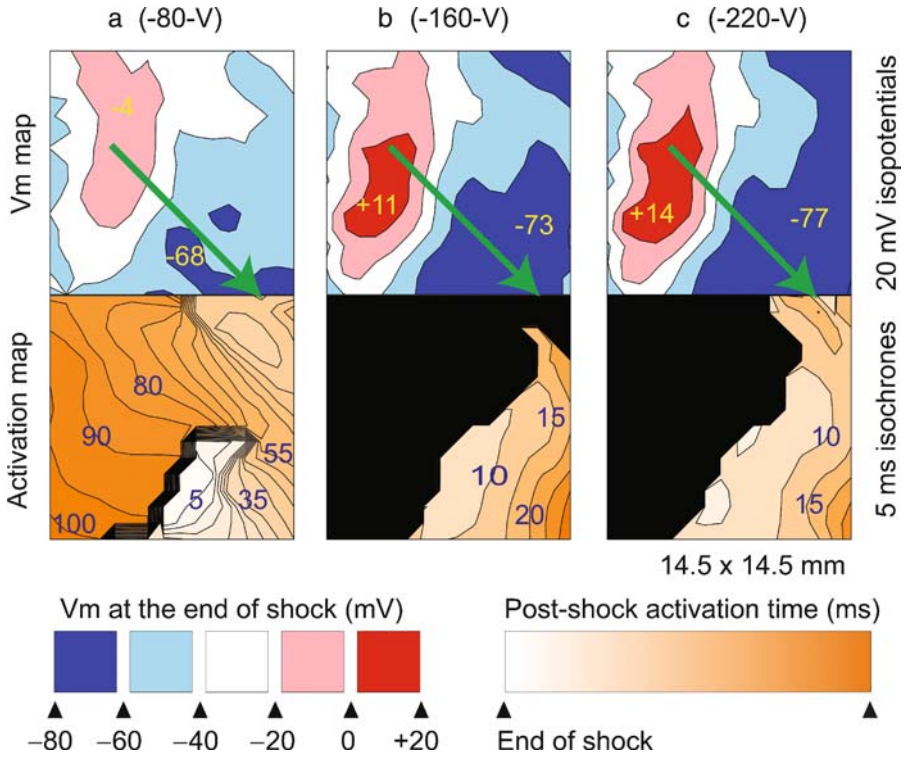

Figure 4: Modulation of virtual electrode polarization (VEP) magnitude and resulting conduction velocity by shock intensity. *Top*: Transmembrane potential at shock end. *Bottom*: Isochronal maps of postshock activation. (**a**–**c**) correspond to shock intensities of −80, −160, and −220 V, respectively (Cheng et al. 1999)[69]

Chirality of Shock-Induced Reentry Predicted by VEP Not the Repolarization Gradient

Frazier and colleagues[59] were the first to experimentally demonstrate the cross-field induced critical point (CFICP) mechanism of reentry induction by point stimulation. This mechanism predicts chirality (direction of rotation) of the induced reentrant circuit based on the directions of the preshock repolarization gradient as well as the applied voltage gradient. Reversal of either direction would result in reversal of chirality. The virtual electrode-induced phase singularity (VEIPS) mechanism,[67] on the other hand, suggests that chirality is predicted by postshock VEP alone and not by the direction of repolarization.

A series of experiments by Cheng et al.[75] successfully demonstrated this hypothesis. An example is shown in Fig. 5. The first two columns show isochronal maps of activation and repolarization, respectively, as a result of pacing from three different locations. The third and fourth columns show pre- and postshock transmembrane potential. As evident from the maps of postshock potential, shock-induced VEP dominates regardless of the

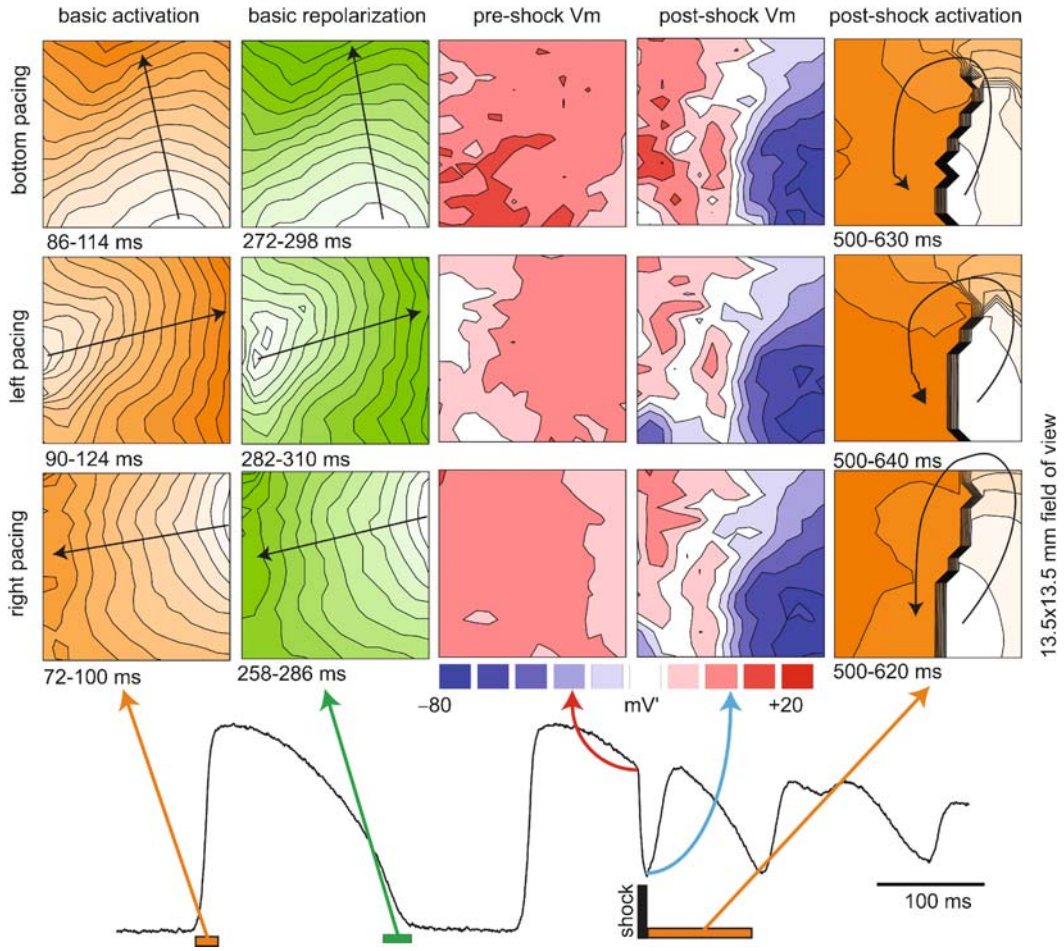

Figure 5: Reentry induced by shocks applied while pacing from three different locations (right ventricle [RV], left ventricle [LV], and apex). Columns from left to right are: activation, repolarization, preshock transmembrane potential, postshock transmembrane potential, and postshock activation. Rows from top to bottom are: apical pacing, RV pacing, and LV pacing. Chirality of shock-induced reentry is preserved regardless of the gradient of repolarization (Cheng et al. 2000)[75]

pattern of repolarization. The last column shows postshock activation with reentry rotating counterclockwise in all cases, thus the data support the VEIPS mechanism and contradict the CFICP hypothesis.

A more detailed analysis of the two mechanisms is shown in Fig. 6. In both panels, a planar wavefront propagates from top to bottom with the transmembrane potential indicated by differing shades of gray. The left panel depicts the CFICP hypothesis and assumes

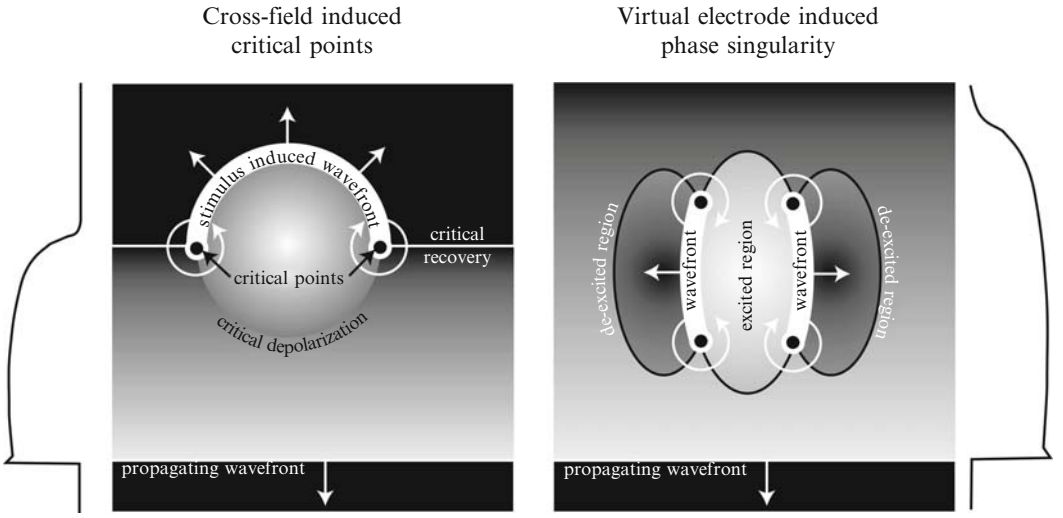

Figure 6: Schematics of the cross-field induced critical point (CFICP) and virtual electrode-induced phase singularity (VEIPS) mechanisms. See text for details (Cheng et al. 2000)[75]

that cathodal point stimulation produces positive polarization near the stimulation site. Two critical values are important in this mechanism: critical recovery, indicated by the line dividing refractory and excitable myocardium at the tail of the action potential, and critical depolarization, indicated with the circle dividing subthreshold from suprathreshold depolarization. The top of the circle of critical depolarization occurs in excitable myocardium, generating a new wavefront. The two points of intersection of critical depolarization and critical recovery represent the sites of wavebreak and are called critical points[59] or points of phase singularity.[73] In this mechanism, reversal of the direction of repolarization will result in wavefront generation along the bottom of the circle of critical depolarization and reversal of chirality.

The VEIPS hypothesis is shown in the right panel of Fig. 6 and predicts that point stimulation will produce regions of adjacent positive and negative polarization. For the case of cathodal stimulation, the stimulation site will be positively polarized (excited) with two negatively polarized (deexcited) regions on either side. The VEIPS mechanism does not rely on existence of an excitable region at the tail of the action potential, as the negatively polarized regions deexcite the tissue, creating an excitable region regardless of repolarization. Two wavefronts will be generated at the areas of adjacent positive and negative polarization, and a total of four wavebreaks or points of phase singularity will be induced. In Fig. 5, only one of the four phase singularities was observed. Reversal of the repolarization gradient can change the location of the two wavefronts of reexcitation, but it will not change their direction. Therefore, chirality will be preserved.

Shock-Induced VEP as a Mechanism for Defibrillation Failure

Thus far, the examples presented have all dealt with shock-induced arrhythmogenesis. However, shock-induced VEP is also present during ventricular arrhythmias and can be responsible for failed defibrillation shocks. Figure 7 illustrates an example of a failed monophasic −100 V defibrillation shock applied from an implantable right ventricle (RV) lead during ventricular tachycardia.[76] By panels 5 and 6, shock-induced VEP completely erases the existing tachycardia. However, due to the strong gradient of VEP, a new reentrant arrhythmia is immediately produced via the VEIPS mechanism.[67] The reentry core of

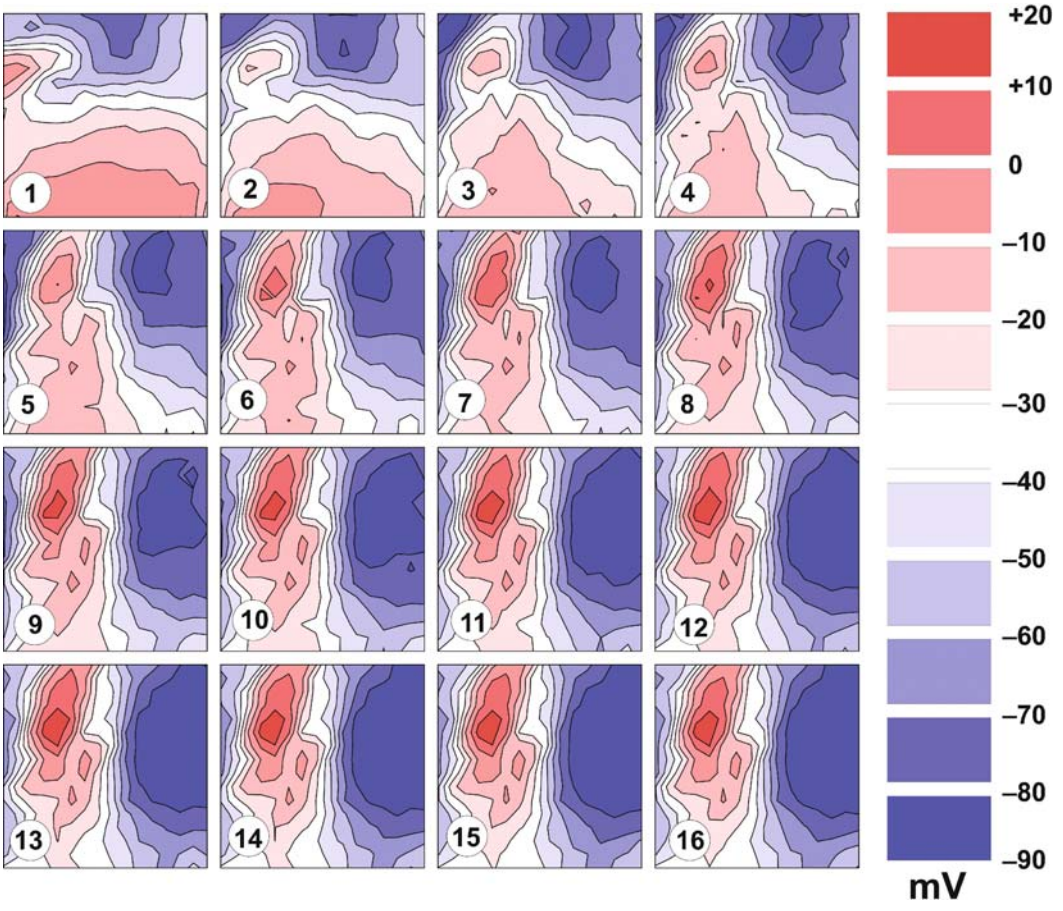

Figure 7: Shock erases ventricular tachycardia via virtual electrode effect. Maps of transmembrane potential during a failed 8 ms monophasic shock. *Panel 1* shows reentrant excitation just before shock application. By *panels 5–6*, reentrant activation is completely erased by typical virtual electrode polarization with simultaneous areas of positive (*red*) and negative (*blue*) polarization (Efimov et al. 2000)[76]

this arrhythmia is distinctly different from the preshock arrhythmia, indicating that the shock terminated the existing arrhythmia and reinitiated a new one, resulting in failed defibrillation.

The Role of Electroporation

Transmembrane polarization produced by virtual electrodes present during a defibrillation shock may reach significant amplitudes, which results in breakdown of the cell membrane.[77,78] This effect is known as *electroporation*. On one hand, electroporation imposes a limit on virtual electrode polarization, due to the formation of low resistance pores, which shunt the transmembrane potential and make it impossible to maintain even the resting potential until the pores are resealed.[78] On the other hand, electroporation may have important electrophysiological implications for arrhythmia maintenance. Experimental evidence suggests that electroporation occurring after a defibrillation shock may result in the creation of new centers of focal activity.[2] However, the pro- and antiarrhythmic effect of electroporation in the clinical setting remains a subject of debate.[1] However, data from implantable defibrillators clearly indicate that spontaneous sinus rhythm does not recover immediately postshock and requires pacing for several seconds. This period of time is consistent with the time course of resealing of electroporated membranes.

Clinical Implications of the Virtual Electrode Hypothesis of Defibrillation

The virtual electrode hypothesis of defibrillation, along with optical mapping techniques, has made great strides toward explaining many experimentally and clinically observed phenomena, which had remained a mystery to scientists and clinicians alike. Many of these discoveries have clinical implications for safe and efficient defibrillation.

The Role of Virtual Electrodes and Shock Polarity

Optical mapping experiments revealed the mechanism of superiority of anodal versus cathodal shocks when applied from transvenous defibrillation leads.[66,79] Figure 8 illustrates the general concept. During anodal shocks (Fig. 8a), the virtual cathodes created adjacent to the real anode produce wavefronts that propagate inward, toward the area of deexcitation. These wavefronts frequently collide and annihilate each other, whereas the positive polarization under the real cathode during cathodal shocks (Fig. 8b) creates wavefronts that propagate outward, having more "elbow room" (in Art Winfree's terms) for turning around and creating sustained reentry. These experimental findings were recently confirmed in a meta-analysis of clinical studies on ICD shock polarity, which revealed that anodal defibrillation shocks lower the defibrillation threshold (DFT) by 14.8% compared to cathodal shocks and result in a lower DFT in 83% of patients.[80] The lower DFT is presumably due to the decreased probability of reinitiating a reentrant arrhythmia postshock.

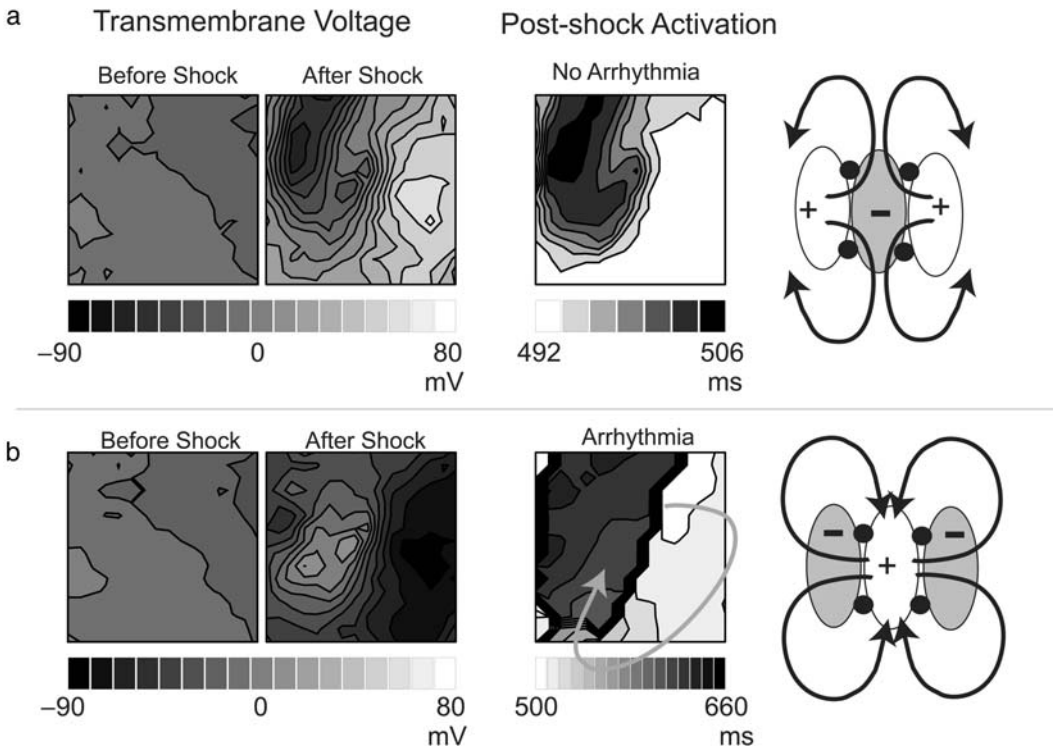

Figure 8: Anodal versus cathodal monophasic defibrillation shocks applied from an implantable lead. (**a**) *Left panels*: Transmembrane potential before and after an anodal shock (+100 V, 8 ms). *Middle*: Spread of postshock activation. The areas of first activation correspond to the virtual cathodes. Activation then spreads to the area of the real anode, collapsing on itself, and no arrhythmia is produced. *Right*: Diagram of postshock activation. (**b**) Similar panels as in (**a**) for a cathodal (−100 V, 8 ms) shock. In this case, activation spreads immediately outward from the real cathode to the virtual anodes where it has room to reenter, creating a sustained arrhythmia (Yamanouchi et al. 2001)[79]

Waveform Optimization

The efficacy of different defibrillation waveforms has also been determined with the virtual electrode hypothesis. It has been widely accepted that biphasic shocks have a lower defibrillation threshold than monophasic shocks,[81,82] but this phenomenon has its roots in the virtual electrode theory. Monophasic shocks must be greater than the ULV in order to avoid creation of a shock-induced phase singularity, which may reinduce reentry. However, the second phase of biphasic shocks acts to reverse the first phase polarization, thus eliminating the substrate for postshock reentry.[67] This phenomenon is illustrated in Fig. 9. The three maps in Fig. 9a show the postshock polarization in response to monophasic (+100 V), optimal biphasic (+100/−50 V), and nonoptimal biphasic

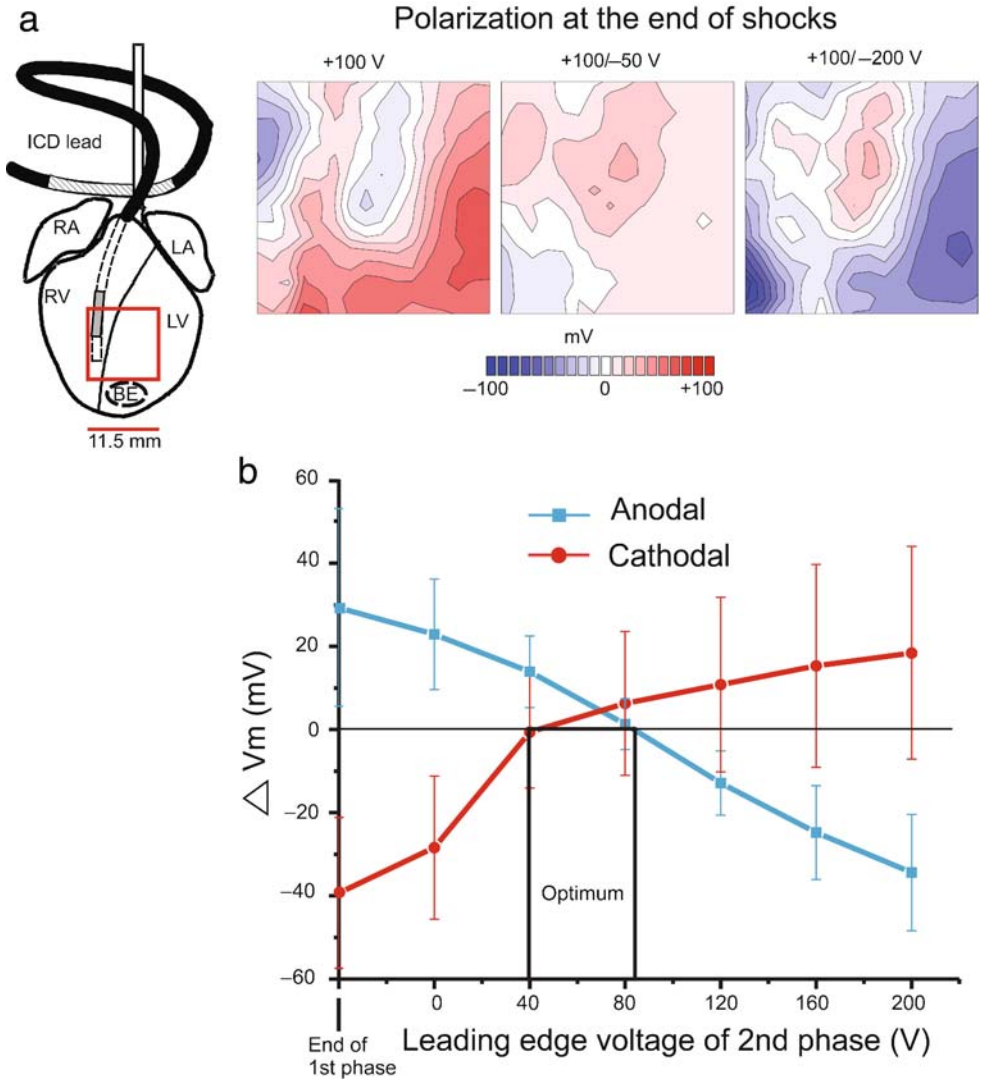

Figure 9: Homogenization of virtual electrode polarization (VEP) by the second phase of biphasic shocks. (**a**) Maps of polarization produced by monophasic (+100 V, 8 ms), optimal biphasic (+100/−50 V, 8/8 ms), and nonoptimal biphasic (+100/−200 V, 8/8 ms) defibrillation shocks. The area of recording is indicated by the *red box*. ICD, implantable cardioverter defibrillator; LA, left atrium; LV, left ventricle; RA, right atrium; RV, right ventricle (Efimov et al. 1998)[67] (**b**) Asymmetric reversal of first-phase polarization. Plot shows gradient of transmembrane potential after second phase of biphasic shocks in which the first phase voltage was held constant and the second phase voltage was varied. Positive polarization produced by anodal first phase was fully reversed by approximately 70 V or more, whereas negative polarization produced by cathodal first phase required only 40 V to reverse

(+100/−200 V) defibrillation shocks. The optimal biphasic shock does not result in reentry due to the homogeneous pattern of VEP at shock end, whereas the large gradient of VEP produced by the monophasic and nonoptimal biphasic waveforms provides the substrate for reentry.

The "homogenization" of VEP by the second phase of a biphasic shock occurs in a nonlinear fashion. After the first phase, the deexcited hyperpolarized region is easily reexcited and completely depolarized, whereas the depolarized regions are only partially deexcited.[67] Therefore, not every biphasic shock will be able to produce this homogenization (Fig. 9a, right panel). If the energy of the second phase is below a certain threshold, it will not be able to reverse the hyperpolarization. If the energy of the second phase is above a certain level, it will reverse both the positive and negative polarization, creating a mirrored VEP pattern similar to a monophasic shock. Efimov et al.[67] found a ratio of between 0.2 and 0.7 of second- versus first-phase voltage for optimal biphasic shocks. This agrees with clinical observations of optimal biphasic waveforms.[82] Figure 9b illustrates these findings and suggests that optimal biphasic waveforms result in total positive polarization with no excitable hyperpolarized tissue remaining to provide the substrate for shock-induced arrhythmias.

Monophasic ascending defibrillation waveforms have also been shown to be superior to descending waveforms.[83] As shown in Fig. 10c, d, ascending waveforms produce maximum polarization at the end of the shock. Therefore, break excitation resulting from these shocks is likely to produce faster propagation into the deexcited regions and will not form reentry (Fig. 10f). However, descending waveforms tend to reach maximum polarization before the end of the shock (Fig. 10c) and typically have lower magnitude polarization at shock end (Fig. 10d), which contributes to slower conduction and provides the substrate for shock-induced reentry via the VEIPS mechanism (Fig. 10f).[67]

Toward Low-Energy Defibrillation

The virtual electrode hypothesis of defibrillation has not only allowed for explanation of the basic mechanisms of defibrillation, but it is also allowing us to entirely rethink our approach to conventional defibrillation. Reentrant VT is often pinned or anchored at a functionally or anatomically heterogeneous region that comprises the core of reentry. The theory of virtual electrode polarization and the activating function predict that areas near the reentry core will experience greater polarization in response to an applied electric field compared to the surrounding, more homogeneous tissue. Thus, the core of reentry can be preferentially excited with very small electric fields to destabilize and unpin reentrant VT from its stationary core. However, the external field must be applied at precisely the right moment for the virtual electrode-induced excitation to properly interact with and terminate VT. This idea has been recently validated both in theory[84] and in experiments.[85,86]

Takagi et al.[84] demonstrated this concept in a two-dimensional bidomain model with a nonconductive circular obstacle comprising the core of reentry. Figure 11 shows a successful and nonsuccessful shock application. At $t = 0$ ms, a spiral wave (S) is shown anchored to the obstacle rotating counterclockwise. A 0.52 V/cm^{-1} uniform external field is applied at

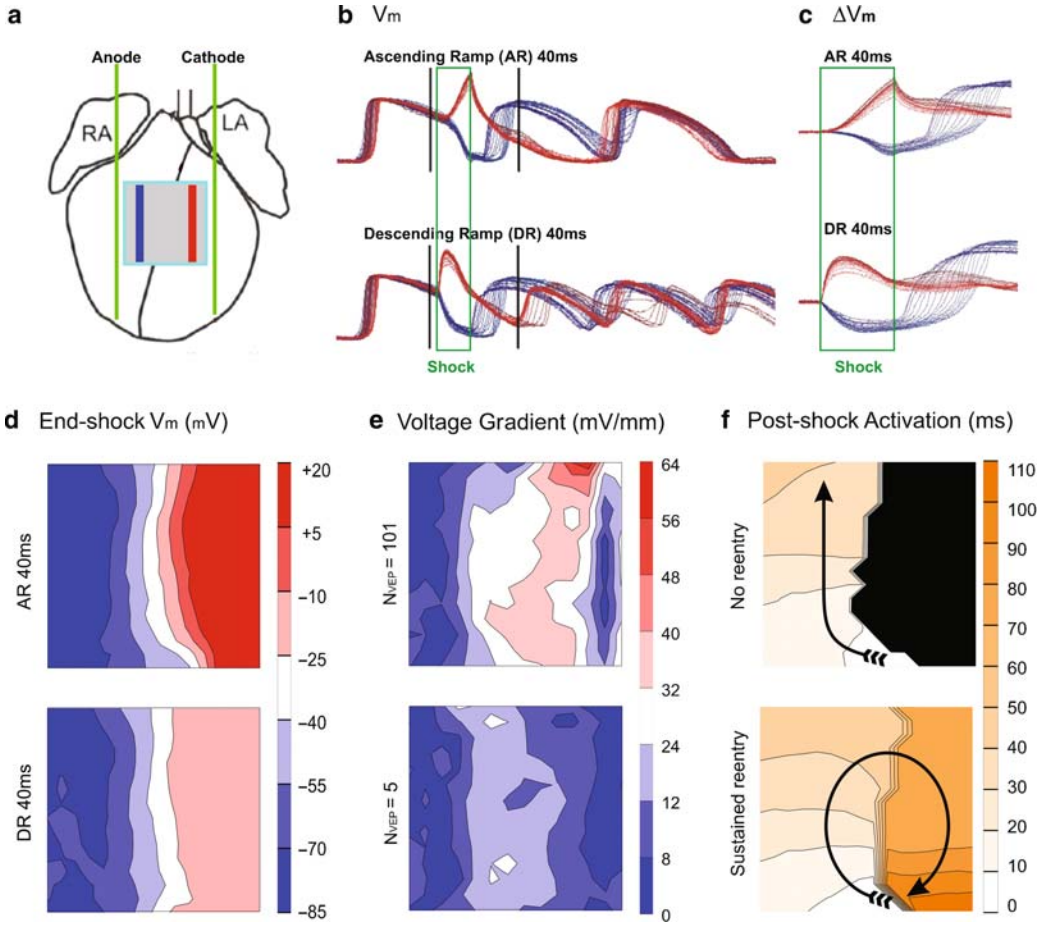

Figure 10: Ascending versus descending ramp monophasic waveforms. (**a**) Schematic of experimental setup showing shock electrode locations (*green lines*), field of view (*blue box*), and locations of individual optical traces shown in (**b**) and (**c**) (*blue and red lines*). RA, right atrium; LA, left atrium. (**b**) Optical action potentials during shock application for ascending and descending ramp defibrillation waveforms. (**c**) ΔV_{m} for the traces shown in (**b**). Ascending waveforms produce maximum polarization at shock end, whereas descending waveforms produce maximum polarization near the beginning of shock application. (**d**) Maps of polarization at shock end. (**e**) Voltage gradient at shock end. (**f**) Maps of postshock activation (Qu et al. 2005)[83]

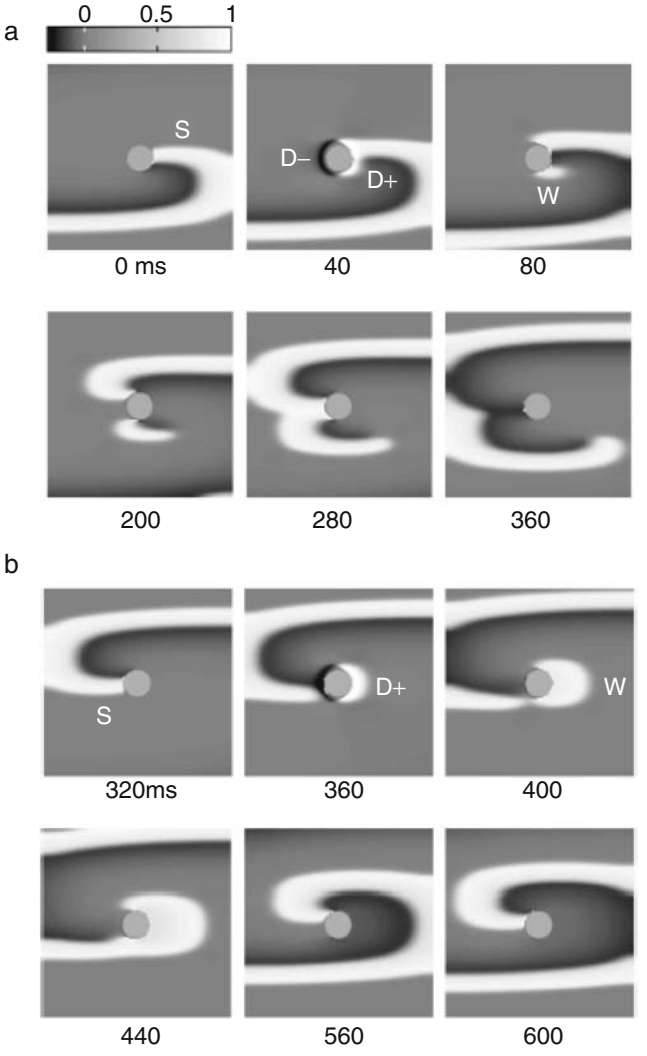

Figure 11: Bidomain simulations illustrating the low-energy "unpinning" concept. (**a**) Successful unpinning. $t = 0$ ms: spiral wave (S) is anchored to the obstacle rotating counterclockwise. $t = 40$ ms: a $0.52\,\mathrm{V/cm^{-1}}$ external field is applied. Positive and negative polarization (D+, D−) occur on opposite sides of the obstacle. $t = 80$ ms: the positive polarization results in a new wavefront (W), which rotates clockwise. $t = 280$ ms: the wavefronts collide resulting in detachment of both spiral waves. (**b**) An unsuccessful attempt due to improper timing of the applied field (Takagi et al. 2004)[84]

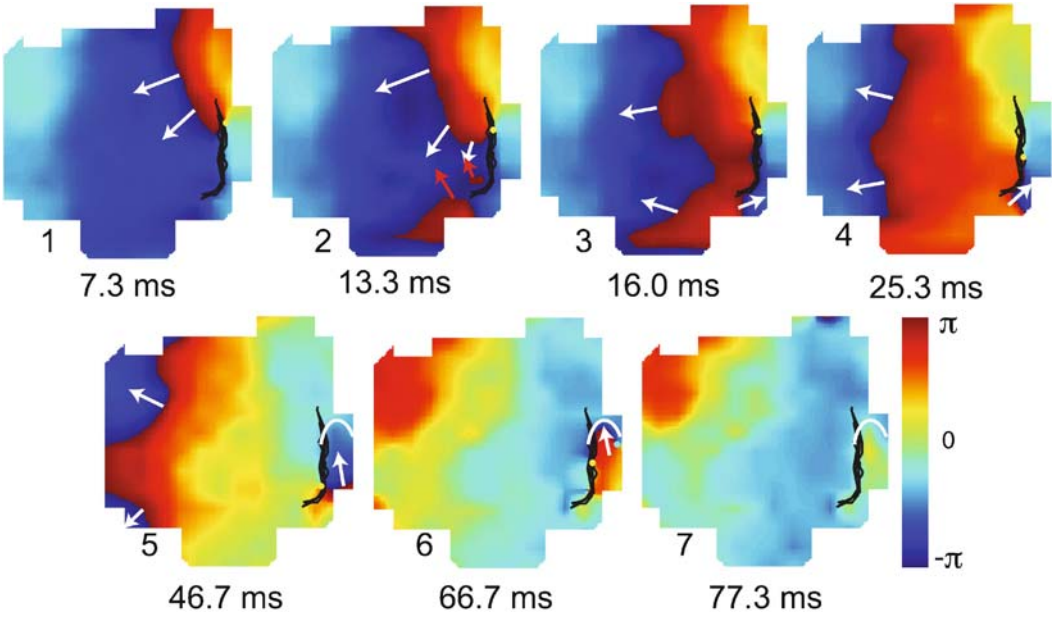

Figure 12: Low-energy unpinning in an isolated rabbit right ventricular free wall preparation. A $0.58\,\mathrm{V/cm^{-1}}$ shock is applied at $t = 13.3\,\mathrm{ms}$. Unpinning is similar to theoretical example presented in Fig. 11. See text for details (Ripplinger et al. 2006)[85]

$t = 40\,\mathrm{ms}$. Positive and negative polarization (D+, D-) can be seen on opposite sides of the obstacle. The positive polarization results in a new wavefront (W), which begins to rotate clockwise around the obstacle. Counterclockwise rotation of W is prevented due to refractory tissue in this direction. The wavefronts collide at $t = 280\,\mathrm{ms}$, which results in detachment of both spiral waves from the obstacle. The lower panels of Fig. 11 illustrate an unsuccessful attempt due to improper timing of the applied field. In this case, W can propagate in both directions and results in resetting of the spiral wave.

Our group recently validated this mechanism experimentally in a rabbit using isolated right ventricular preparation.[85] Figure 12 shows a spiral wave rotating counterclockwise around a line of block indicated with a black line (panel 1). At $t = 13.3\,\mathrm{ms}$, a $0.58\,\mathrm{V/cm^{-1}}$ external field is applied, creating a new wavefront that propagates in both directions around the line of block. The clockwise-propagating wavefront then collides with the existing spiral wave (panel 3) causing detachment from the core and termination at the tissue boundary (panels 4–5). The counterclockwise portion of the new wavefront eventually terminates upon hitting a refractory region (panel 6–7). Our experimental results in this model indicate that a 20-fold reduction in defibrillation energy may be obtained compared to conventional defibrillation. In a follow-up study, our group demonstrated a similar 20-fold reduction in defibrillation energy required to terminate sustained VT in a canine 4-day healed myocardial infarction model.[86] This new low energy approach may provide a promising alternative to

conventional high-energy defibrillation and may alleviate many of the side effects currently associated with strong electric shocks.

Conclusion

The virtual electrode hypothesis of defibrillation has emerged as a result of the combined efforts of the theoretical and experimental research communities, which have developed bidomain modeling and optical mapping. These two research methodologies have allowed us to formulate novel hypotheses and to test them in various models of defibrillation. However, clinical advances are still to be gained from this theory. We believe that further improvement of the virtual electrode hypothesis of defibrillation will result in the development of low-energy electrotherapy of ventricular and atrial tachyarrhythmias.

References

1. Al Khadra A, Nikolski V, Efimov IR. The role of electroporation in defibrillation. *Circ Res* 2000;87(9):797–804
2. Kodama I, Shibata N, Sakuma I, Mitsui K, Iida M, Suzuki R, Fukui Y, Hosoda S, Toyama J. Aftereffects of high-intensity DC stimulation on the electromechanical performance of ventricular muscle. *Am J Physiol* 267(1 Pt 2):H248–H258
3. Neunlist M, Tung L. Dose-dependent reduction of cardiac transmembrane potential by high-intensity electrical shocks. *Am J Physiol* 273(6 Pt 2):H2817–H2825
4. Godemann F, Butter C, Lampe F, Linden M, Schlegl M, Schultheiss HP, Behrens S. Panic disorders and agoraphobia: side effects of treatment with an implantable cardioverter/defibrillator. *Clin Cardiol* 27(6):321–326
5. Kamphuis HC, de Leeuw JR, Derksen R, Hauer RN, Winnubst JA. Implantable cardioverter defibrillator recipients: quality of life in recipients with and without ICD shock delivery: a prospective study. *Europace* 5(4):381–389
6. Fye WB. Ventricular fibrillation and defibrillation: historical perspectives with emphasis on the contributions of John MacWilliam, Carl Wiggers, and William Kouwenhoven. *Circ* 1985;71(5):858–865
7. Prevost JL, Battelli F. Sur quel ques effets des dechanges electriques sur le coer mammifres. *C R Seances Acad Sci* 1899;129:1267
8. Gurvich NL, Yuniev GS. Restoration of regular rhythm in the mammalian fibrillating heart. *Am Rev Sov Med* 1946;3:236–239
9. Beck CS, Pritchard WH, Feil HS. Ventricular fibrillation of long duration abolished by electric shock. *JAMA* 1947;135:985
10. Zoll PM, Linethal AJ, Gibson W, et al. Termination of ventricular fibrillation in man by externally applied electric shock. *N Engl J Med* 1956;254:727
11. Kouwenhoven WB, Milnor WR. Treatment of ventricular fibrillation using a capacitor discharge. *J Appl Physiol* 1954;7(3):253–257

12. Lown B, Neuman J, Amarasingham R, Berkovits BV. Comparison of alternating current with direct electroshock across the closed chest. *Am J Cardiol* 1962;10:223–233
13. Gurvich NL. *The Main Principles of Cardiac Defibrillation*. Moscow: Medicine; 1975
14. Mirowski M, Mower MM, Reid PR. The automatic implantable defibrillator. *Am Heart J* 1980;100(6 Pt 2):1089–1092
15. Mirowski M, Reid PR, Mower MM, Watkins L, Gott VL, Schauble JF, Langer A, Heilman MS, Kolenik SA, Fischell RE, Weisfeldt ML. Termination of malignant ventricular arrhythmias with an implanted automatic defibrillator in human beings. *N Engl J Med* 1980;303(6):322–324
16. Tung L. *A Bidomain Model for Describing Ischemia Myocardial DC Potentials*. Cambridge, MA: Massachusetts Institute of Technology; 1978
17. Henriquez CS. Simulating the electrical behavior of cardiac tissue using the bidomain model. *Crit Rev Biomed Eng* 1993;21(1):1–77
18. Skouibine K, Trayanova N, Moore P. A numerically efficient model for simulation of defibrillation in an active bidomain sheet of myocardium. *Math Biosci* 2000;166(1):85–100
19. Krassowska W. Effects of electroporation on transmembrane potential induced by defibrillation shocks. *Pacing Clin Electrophysiol* 1995;18(9 Pt 1):1644–1660
20. Beeler GW, Reuter H. Reconstruction of the action potential of ventricular myocardial fibres. *J Physiol (Lond)* 1977;268(1):177–210
21. Drouhard JP, Roberge FA. A simulation study of the ventricular myocardial action potential. *IEEE Trans Biomed Eng* 1982;29(7):494–502
22. Luo CH, Rudy Y. A model of the ventricular cardiac action potential. Depolarization, repolarization, and their interaction. *Circ Res* 1991;68(6):1501–1526
23. Luo CH, Rudy Y. A dynamic model of the cardiac ventricular action potential. I. Simulations of ionic currents and concentration changes. *Circ Res* 1994;74(6):1071–1096
24. Hund TJ, Rudy Y. Rate dependence and regulation of action potential and calcium transient in a canine cardiac ventricular cell model. *Circulation* 2004;110(20):3168–3174
25. Hodgkin AL, Huxley AF. Propagation of electrical signals along giant nerve fibers. *Proc R Soc Lond B Biol Sci* 1952;140(899):177–183
26. Cohen LB, Lesher S, De Weer P, Salzberg BM. Optical monitoring of membrane potential: methods of multisite optical measurement. *Optical Methods in Cell Physiology*. New York: Wiley-Interscience; 1986:71–100
27. Davila HV, Salzberg BM, Cohen LB, Waggoner AS. A large change in axon fluorescence that provides a promising method for measuring membrane potential. *Nat New Biol* 1973;241(109):159–160
28. Salama G, Morad M. Merocyanine 540 as an optical probe of transmembrane electrical activity in the heart. *Science* 1976;191(4226):485–487
29. Morad M, Salama G. Optical probes of membrane potential in heart muscle. *J Physiol (Lond)* 1979;292:267–295
30. Ross WN, Salzberg BM, Cohen LB, Grinvald A, Davila HV, Waggoner AS, Wang CH. Changes in absorption, fluorescence, dichroism, and birefringence in stained giant axons: optical measurement of membrane potential. *J Membr Biol* 1977;33(1–2):141–183

31. Salama G, Loew LM. Optical measurements of transmembrane potential in heart. *Spectroscopic Membrane Probes*. Boca Raton, FL: CRC; 1988:137–199
32. Dillon S, Morad M. A new laser scanning system for measuring action potential propagation in the heart. *Science* 1981;214(4519):453–456
33. Kodama I, Sakuma I, Shibata N, Knisley SB, Niwa R, Honjo H. Regional differences in arrhythmogenic aftereffects of high intensity DC stimulation in the ventricles. *Pacing Clin Electrophysiol* 2000;23(5):807–817
34. Entcheva E, Kostov Y, Tchernev E, Tung L. Fluorescence imaging of electrical activity in cardiac cells using an all-solid-state system. *IEEE Trans Biomed Eng* 2004;51(2):333–341
35. Amino M, Yamazaki M, Nakagawa H, Honjo H, Okuno Y, Yoshioka K, Tanabe T, Yasui K, Lee JK, Horiba M, Kamiya K, Kodama I. Combined effects of nifekalant and lidocaine on the spiral-type re-entry in a perfused 2-dimensional layer of rabbit ventricular myocardium. *Circ J* 2005;69(5):576–584
36. Bray MA, Lin SF, Wikswo JP. Panoramic epifluorescent visualization of cardiac action potential activity. *Proc SPIE* 1999;3658:99–107
37. Lin SF, Wikswo JP. Panoramic optical imaging of electrical propagation in isolated heart. *J Biomed Opt* 1999;4(2):200–207
38. Bray MA, Lin SF, Wikswo J. Three-dimensional visualization of phase singularities on the isolated rabbit heart. *J Cardiovasc Electrophysiol* 2002;13(12):1311
39. Kay MW, Amison PM, Rogers JM. Three-dimensional surface reconstruction and panoramic optical mapping of large hearts. *IEEE Trans Biomed Eng* 2004;51(7):1219–1229
40. Qu F, Ripplinger CM, Nikolski VP, Grimm C, Efimov IR. Three dimensional panoramic imaging of cardiac arrhythmias in the rabbit heart. *J Biomed Opt* 2007;12(4):044019
41. Furman S, Hurzeler P, Parker B. Clinical thresholds of endocardial cardiac stimulation: a long-term study. *J Surg Res* 1975;19:149–155
42. Rattay F. Analysis of models for extracellular fiber stimulation. *IEEE Trans Biomed Eng* 1989;36(7):676–682
43. Sobie EA, Susil RC, Tung L. A generalized activating function for predicting virtual electrodes in cardiac tissue. *Biophysical J* 1997;73(3):1410–1423
44. Sepulveda NG, Roth BJ, Wikswo JP. Current injection into a two-dimensional anisotropic bidomain. *Biophysical J* 1989;55(5):987–999
45. Wikswo JP, Lin SF, Abbas RA. Virtual electrodes in cardiac tissue: a common mechanism for anodal and cathodal stimulation. *Biophysical J* 1995;69(6):2195–2210
46. Fast VG, Rohr S, Gillis AM, Kleber AG. Activation of cardiac tissue by extracellular electrical shocks: formation of 'secondary sources' at intercellular clefts in monolayers of cultured myocytes. *Circ Res* 1998;82(3):375–385
47. Trayanova N, Skouibine K, Aguel F. The role of cardiac tissue structure in defibrillation. *Chaos* 1998;8(1):221–233
48. Gurvich NL, Yuniev GS. Restoration of regular rhythm in the mammalian fibrillating heart. *Byull Eksper Biol Med* 1939;8(1):55–58

49. Zipes DP, Fischer J, King RM, Nicoll Ad, Jolly WW. Termination of ventricular fibrillation in dogs by depolarizing a critical amount of myocardium. *Am J Cardiol* 1975;36(1):37–44
50. Witkowski FX, Penkoske PA, Plonsey R. Mechanism of cardiac defibrillation in open-chest dogs with unipolar DC-coupled simultaneous activation and shock potential recordings. *Circulation* 1990;82(1):244–260
51. Krinskii VI, Fomin SV, Kholopov AV. [Critical mass during fibrillation]. *Biofizika* 1967;12(5):908–914
52. Fabiato A, Coumel P, Gourgon R, Saumont R. The threshold of synchronous response of the myocardial fibers. Application to the experimental comparison of the efficacy of different forms of electroshock defibrillation. *Arch Mal Coeur Vaiss* 1967;60(4):527–544
53. Chen PS, Shibata N, Dixon EG, Martin RO, Ideker RE. Comparison of the defibrillation threshold and the upper limit of ventricular vulnerability. *Circulation* 1986;73(5):1022–1028
54. Shibata N, Chen PS, Dixon EG, Wolf PD, Danieley ND, Smith WM, Ideker RE. Influence of shock strength and timing on induction of ventricular arrhythmias in dogs. *Am J Physiol* 1988;255(4 Pt 2):H891–H901
55. Fabritz CL, Kirchhof PF, Behrens S, Zabel M, Franz MR. Myocardial vulnerability to T wave shocks: relation to shock strength, shock coupling interval, and dispersion of ventricular repolarization. *J Cardiovasc Electrophysiol* 1996;7(3):231–242
56. Chen PS, Feld GK, Kriett JM, Mower MM, Tarazi RY, Fleck RP, Swerdlow CD, Gang ES, Kass RM. Relation between upper limit of vulnerability and defibrillation threshold in humans. *Circulation* 1993;88(1):186–192
57. Hwang C, Swerdlow CD, Kass RM, Gang ES, Mandel WJ, Peter CT, Chen PS. Upper limit of vulnerability reliably predicts the defibrillation threshold in humans. *Circulation* 1994;90(5):2308–2314
58. Wiener N, Rosenblueth A. The mathematical formulation of the problem of conduction of impulses in a network of connected excitable elements, specifically in cardiac muscle. *Arch Inst Cardiol Mexico* 1946;16(3–4):205–265
59. Frazier DW, Wolf PD, Wharton JM, Tang AS, Smith WM, Ideker RE. Stimulus-induced critical point. Mechanism for electrical initiation of reentry in normal canine myocardium. *J Clin Invest* 1989;83(3):1039–1052
60. Walcott GP, Walcott KT, Knisley SB, Zhou X, Ideker RE. Mechanisms of defibrillation for monophasic and biphasic waveforms. *Pacing Clin Electrophysiol* 1994;17(3 Pt 2):478–498
61. Walcott GP, Walcott KT, Ideker RE. Mechanisms of defibrillation. Critical points and the upper limit of vulnerability. *J Electrocardiol* 1995;28(Suppl):1–6
62. Dillon SM, Kwaku KF. Progressive depolarization: a unified hypothesis for defibrillation and fibrillation induction by shocks. *J Cardiovasc Electrophysiol* 1998;9(5):529–552
63. Roth BJ. A mathematical model of make and break electrical stimulation of cardiac tissue by a unipolar anode or cathode. *IEEE Trans Biomed Eng* 1995;42(12):1174–1184
64. Knisley SB, Hill BC, Ideker RE. Virtual electrode effects in myocardial fibers. *Biophysical J* 1994;66(3 Pt 1):719–728

65. Neunlist M, Tung L. Spatial distribution of cardiac transmembrane potentials around an extracellular electrode: dependence on fiber orientation. *Biophysical J* 1995;68(6):2310–2322
66. Efimov IR, Cheng YN, Biermann M, Van Wagoner DR, Mazgalev T, Tchou PJ. Transmembrane voltage changes produced by real and virtual electrodes during monophasic defibrillation shock delivered by an implantable electrode. *J Cardiovasc Electrophysiol* 1997;8:1031–1045
67. Efimov IR, Cheng Y, Van Wagoner DR, Mazgalev T, Tchou PJ. Virtual electrode-induced phase singularity: a basic mechanism of defibrillation failure. *Circ Res* 1998;82(8):918–925
68. Efimov IR, Gray RA, Roth BJ. Virtual electrodes and de-excitation: new insights into fibrillation induction and defibrillation. *J Cardiovasc Electrophysiol* 2000;11(3):339–353
69. Cheng Y, Mowrey KA, Van Wagoner DR, Tchou PJ, Efimov IR. Virtual electrode induced re-excitation: a basic mechanism of defibrillation. *Circ Res* 1999;85(11):1056–1066
70. Hoffa M, Ludwig C. Einige neue Versuche uber Herzbewegung. *Zeitschrift Rationelle Medizin* 1850;9:107–144
71. Skouibine K, Trayanova NA, Moore P. Anode/cathode make and break phenomena in a model of defibrillation. *IEEE Trans Biomed Eng* 1999;46(7):769–777
72. Lin SF, Roth BJ, Wikswo JP. Quatrefoil reentry in myocardium: an optical imaging study of the induction mechanism. *J Cardiovasc Electrophysiol* 1999;10:574–586
73. Winfree AT. *When Time Breaks Down: The Three-Dimensional Dynamics of Electrochemical Waves and Cardiac Arrhythmias*. Princeton, NJ: Princeton University Press; 1987
74. Cheng Y, Van Wagoner D, Tchou PJ, Efimov IR. Defibrillation shock-induced waves of re-excitation: implications to upper and lower limits of vulnerability. *PACE* 1999;22(4(II)):809
75. Cheng Y, Nikolski V, Efimov IR. Reversal of repolarization gradient does not reverse the chirality of shock-induced reentry in the rabbit heart. *J Cardiovasc Electrophysiol* 2000;11(9):998–1007
76. Efimov IR, Cheng Y, Yamanouchi Y, Tchou PJ. Direct evidence of the role of virtual electrode induced phase singularity in success and failure of defibrillation. *J Cardiovasc Electrophysiol* 2000;11(8):861–868
77. Jones JL, Jones RE, Balasky G. Microlesion formation in myocardial cells by high-intensity electric field stimulation. *Am J Physiol* 1987;253(2 Pt 2):H480–H486
78. Nikolski VP, Sambelashvili AT, Krinsky VI, Efimov IR. Effects of electroporation on optically recorded transmembrane potential responses to high-intensity electrical shocks. *Am J Physiol Heart Circ Physiol* 2004;286(1):H412–H418
79. Yamanouchi Y, Cheng Y, Tchou PJ, Efimov IR. The mechanisms of vulnerable window: the role of virtual electrodes and shock polarity. *Can J Physiol Pharmacol* 2001;79(1):25–33
80. Kroll MW, Efimov IR, Tchou PJ. Present understanding of shock polarity for internal defibrillation: the obvious and non-obvious clinical implications. *Pacing Clin Electrophysiol* 2006;29(8):885–891

81. Chapman PD, Vetter JW, Souza JJ, Troup PJ, Wetherbee JN, Hoffmann RG. Comparative efficacy of monophasic and biphasic truncated exponential shocks for nonthoracotomy internal defibrillation in dogs. *J Am Coll Cardiol* 1988;12(3):739–745
82. Feeser SA, Tang AS, Kavanagh KM, Rollins DL, Smith WM, Wolf PD, Ideker RE. Strength-duration and probability of success curves for defibrillation with biphasic waveforms. *Circulation* 1990;82(6):2128–2141
83. Qu F, Li L, Nikolski VP, Sharma V, Efimov IR. Mechanisms of superiority of ascending ramp waveforms: new insights into mechanisms of shock-induced vulnerability and defibrillation. *Am J Physiol Heart Circ Physiol* 2005;289(2):H569–H577
84. Takagi S, Pumir A, Pazo D, Efimov I, Nikolski V, Krinsky V. Unpinning and removal of a rotating wave in cardiac muscle. *Phys Rev Lett* 2004;93(5):058101
85. Ripplinger CM, Krinsky VI, Nikolski VP, Efimov IR. Mechanisms of unpinning and termination of ventricular tachycardia. *Am J Physiol Heart Circ Physiol* 2006;291(1):H184–H192
86. Fedorov VV, Schuessler RB, Lall S, Ripplinger CM, Sakamoto S, Efimov IR. Low voltage defibrillation of sustained ventricular tachycardia in infarcted canine hearts. *Heart Rhythm* 2007;4 (5S):S171

http://www.springer.com/978-0-387-79402-0

Cardiac Bioelectric Therapy
Mechanisms and Practical Implications
Efimov, I.R.; Kroll, M.W.; Tchou, P. (Eds.)
2009, XXIII, 634 p., Hardcover
ISBN: 978-0-387-79402-0